Integrated Generator-Rectifier Co-Design for Offshore Wind Turbines

Phuc Huynh, Samith Sirimanna, Jay Mok, Dongsu Lee, Olaolu Ajala, Sara Linares, Daniel Mulas, Kiruba Haran, Alejandro Dominguez-Garcia, George Gross, Arijit Banerjee
Department of Electrical and Computer Engineering,
University of Illinois, Urbana, IL, USA

***Abstract*—Harvesting offshore wind energy conventionally relies on multi-megawatt direct-drive permanent-magnet synchronous generators equipped with full-power-rated active rectifiers. Functional integration of the generator and rectifier has led to the creation of an integrated generator-rectifier system with higher efficiency, reliability and power density. In this architecture, power electronics weight and efficiency depend on the generator inductance, while at the same time, the generator design must be optimized for weight and efficiency to realize the potential system-level benefits. This paper proposes a framework using the generator per-unit reactance as a handshake variable to co-design the generator and power electronics. The design approach enables the reduction of the system weight and conversion losses by 25% and 61%, respectively, for a 10-MW system. Using conservative assumptions, economic and reliability assessments show a 4.5% increase in annual energy production, a 9x reduction in long-term failure rate, and a 6.5% decrease in levelized cost of electricity.**

I. Introduction

Offshore wind has emerged as a critical renewable energy resource with a massive untapped potential [1]. Currently, this resource has a relatively high levelized cost of electricity (LCOE) compared to other alternatives such as onshore wind and solar [2]. Creation of an efficient, compact, and reliable electromechanical energy-conversion system is imperative to reduce the LCOE. An integrated generator-rectifier architecture has been shown to be more attractive than other conventional architectures [3]–[6].

The integrated generator-rectifier architecture is shown in Fig. 1 [5]. A multi-port permanent-magnet synchronous generator is used to convert mechanical to electrical power. To convert ac waveforms at the generator terminal to regulated dc, all-but-one ports of the generator are connected to passive rectifiers. Windings in these ports are phase-shifted to reduce the dc-side voltage ripple, eliminating the need for a dc filter capacitor and, consequently, high ac-side power factor is achieved. For simplicity, all the passive ports are collectively represented as one passive rectifier section in Fig. 1. The remaining port connects to an active rectifier controlling the total generator power flow to achieve maximum power-point tracking for the turbine [7]. As most of the power is processed by the diode-based passive rectifier, the integrated system operates efficiently and reliably, while achieving high power density. These attributes open up opportunities to reduce the LCOE.

The generator inductance for the passive and active rectifier sections, denoted by L_p and L_a, respectively, in Fig. 1, are critical design parameters which strongly influence the system power density and efficiency. For example, the presence of

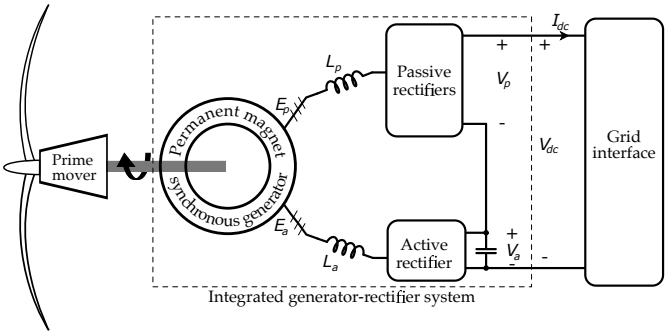

Figure 1. An integrated generator-rectifier system [5]. Mechanical power on the prime-mover shaft is converted to ac electrical power by a multi-port PMSG, and then to dc electrical power by serially-stacked passive and active rectifiers.

L_p manifests as a commutation voltage drop in the passive rectifier section. A high L_p creates non-uniformity in the generator current densities between the active and passive rectifier sections. In contrast, a lower L_a increases the ripple current at the switching frequency and, as a result, the total harmonic distortion for the active rectifier. Further, from a generator-design perspective, a demand for a specific generator inductance influences the selection of the generator topology as well as adding another constraint to the efficiency-versus-weight trade off. Unlike conventional systems, the generator and power electronics design becomes inter-dependent, creating the need for a co-design framework.

This paper presents the co-design framework for the integrated generator-rectifier system. The design objective is to minimize the combined weight and maximize the overall efficiency of the power electronics and the generator. The generator inductance is used as the shared decision variable to pair the generator and power electronic designs. The framework results in feasible generator-rectifier systems that are up to 25-ton lighter and 61% less lossy compared to the conventional solutions for a 10 MW wind turbine. The framework is subsequently expanded to estimate the LCOE for all compatible designs using

$$LCOE = \frac{\varphi.c_f + c_{O\&M}}{\epsilon} \tag{1}$$

where φ is capital recovery factor, c_f the fixed cost, $c_{O\&M}$ operational and maintenance (O&M) cost, and ϵ annual energy production (AEP). An economic assessment as well as a reliability analysis are included to make this LCOE estimation

meaningful. The proposed architecture achieves a 9x reduction in the long-term failure rate and a 4.5% increase in AEP that gives a reduction of LCOE by 6.5%, under conservative assumptions.

The rest of the paper is organized as follows: Section II elaborates the co-design framework including generator and rectifier design. A co-design for a 10-MW offshore wind turbine system is illustrated in Section III. Additional assessments, including annual energy production, reliability, and LCOE are presented in Section IV to provide a metric space for design selection and comparison.

II. Co-design Framework

A conventional approach typically pre-defines the terminal voltage to ensure the compatibility between the generator and the power electronics designs. In contrast, the proposed co-design framework employs the per-unit generator reactance X_L^{pu} as a *handshake* variable, shown in Fig. 2. An initial generator-design block outputs a per-unit reactance. This reactance is utilized in the power electronics design to compute a split ratio that minimizes the active-rectifier volt-ampere (VA) rating. The split ratio divides the total generator number of turns into two sections, one connects to the passive rectifiers and the other to the active rectifier. An available switch voltage rating is used to calculate the actual dc-bus voltage and the required generator back emf. In the final generator design step, the number of turns per phase is determined to match the actual back emf with the power electronics requirement. Finally, the co-design outputs are compared using a design assessment step, in which the weight, efficiency, cost, and power processed by the active rectifier along with a wind profile and additional fixed costs are used to estimate the AEP, failure rate, O&M cost, and LCOE.

A. Generator per-unit reactance X_L^{pu}

As the generator is connected to two different rectifier sections, shown in Fig. 1, a split ratio k is used to denote the relative share of the generator windings for each section. The split ratio is defined by

$$k = \frac{E_a}{E_a + E_p} \tag{2}$$

where, E_a and E_p are the peak line-to-neutral back emfs for the active and passive sections, respectively, at the rated generator speed. The sum of E_a and E_p is the total generator back emf, E. For normalization, the base voltage V_{base} and the base power P_{base} are chosen as

$$V_{base} = \frac{E\sqrt{3}}{\sqrt{2}} \text{ and } P_{base} = P_{rated} \tag{3}$$

where P_{rated} is rated power of the wind turbine. The generator per-phase total inductance L is the sum of L_a and L_p and is represented in per-unit reactance as

$$X_L^{pu} = \frac{\omega L P_{base}}{V_{base}^2} \tag{4}$$

where ω is the generator rated speed.

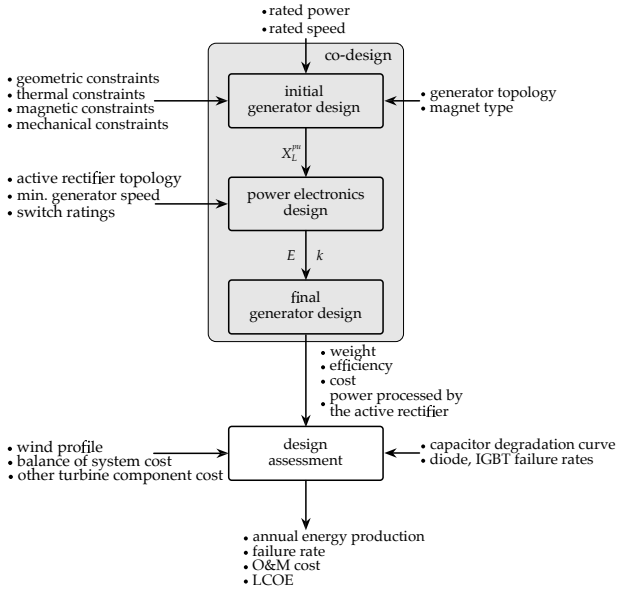

Figure 2. Proposed co-design framework based on per-unit generator reactance X_{pu}^L as a *handshake* parameter between generator and power electronics designs.

B. X_L^{pu} is the handshake variable between the generator and power electronics

Each phase of the generator is constructed by serially connecting individual coils belonging to a magnetic pole pair. As shown in (3), the base voltage is set by the total generator rated back emf and, therefore, is proportional to the number of turns per pole per phase, denoted by N. The generator inductance L is proportional to N^2, which makes X_L^{pu} independent of N as seen in (4). Consequently, X_L^{pu} and E are also independent, allowing an assumption of a hypothetical back emf for the initial generator design stage, as detailed in Section II-C. Knowledge of X_L^{pu} from the generator design stage, along with minimum generator speed, ω_{min}^{pu}, and the switch voltage rating, are sufficient to complete the design process for the power electronics, as detailed in Section II-D. Lastly, the number of turns N to match the back emf requirement from the power electronics is accounted for in the final generator design stage.

C. Initial generator design

The objective at the initial generator design stage is to establish the weight-efficiency Pareto front and compute the X_L^{pu} for individual designs. The input to this stage includes rated power, rated speed, number of poles, and airgap length. A multi-objective optimization problem is formulated based on the selected generator topology and magnet type, along with geometric, thermal, magnetic, and mechanical constraints. The generator dimensions are the decision variables, which are bounded based on practical limitations and/or experience. Mathematically,

$$\begin{aligned} \underset{J, x_i, i=1\ldots k}{\text{maximize}} \quad & \eta_g,\ \frac{1}{m_g} \\ \text{subject to} \quad & b_{il} \le x_i \le b_{iu},\ i = 1\ldots k \\ & J_l \le J \le J_u; \end{aligned} \tag{5}$$

where η_g is the generator rated efficiency, m_g is generator active weight, x_i are the geometric variables having lower bound b_{il} and upper bound b_{iu}, J is the slot current density with the lower bound J_l and upper bound J_u. In addition, the stator flux density is kept below a saturation limit. The multi-objective optimization is solved to generate the Pareto front by using a combination of finite element analysis (FEA) tools and optimization algorithms.

As an example, *Flux*™ in conjunction with *GOSET* [8] are employed to create the trade-off curve. The FEA model in *Flux*™ is constructed using geometric variables to estimate the torque output for a stack length of one meter as well as the iron flux density. The flux density is applied to estimate the generator iron loss using Steinmetz equations. Generator copper loss is calculated employing the current density and the copper area assuming a steady-state temperature of 120 °C. End winding length is estimated using the generator pole pitch, which is used as a correction factor for the total copper loss. The generator stack length is scaled to match the rated power output and, consequently, the active weight is estimated. Efficiency is computed based on the loss calculation and the rated power. The active weight and efficiency are then fed to the *GOSET* algorithm to generate new values for the geometric variables to be used for the next iteration. An additional FEA simulation is performed at each design iteration to evaluate the generator phase-winding self inductance, which is converted to X_L^{pu} using (4) and a hypothetical back emf.

D. Power electronics design

Minimizing the VA rating of the active rectifier, *defined as product of the maximum dc-side voltage and the maximum ac-side current*, is critical due to correlation to the rectifier size, weight, and cost [5]. Minimization is achieved by choosing the split ratio.

The active rectifier dc-side voltage V_a is set by the dc-bus voltage V_{dc} and by the passive-rectifier dc-side voltage V_p, as shown in Fig. 1, given by

$$V_a = V_{dc} - V_p. \tag{6}$$

V_{dc} is assumed to be maintained by a grid-side converter in an ac-collection system, or by a converter at the substation in a dc-collection grid. V_{dc} is expressed in terms of the base voltage as

$$V_{dc} = (1+\alpha)V_{base}\sqrt{2} \tag{7}$$

where α is a design parameter that ensures the active rectifier has a sufficient dc-side voltage relative to the back emf. V_p is dependent on the generator speed and is given by

$$V_p(\omega^{pu}) = \frac{3}{\pi}\sqrt{3}\omega^{pu}E_p - \frac{3}{\pi}\omega^{pu}\omega L_p I_{dc}(\omega^{pu}) \tag{8}$$

where ω^{pu} is the per-unit generator speed, ω is the rated electrical frequency, and I_{dc} is the dc-bus current. This relationship assumes a sufficiently small synchronous inductance L_p such that the passive rectifiers operate in Mode I [9]. The dc-bus current is proportional to cube of the generator speed to achieve MPPT, which in per-unit form is

$$I_{dc}(\omega^{pu}) = (\omega^{pu})^3 \frac{P_{base}}{V_{dc}}. \tag{9}$$

Substituting (7), (8) and (9) into (6), then normalizing both sides by V_{base} and using (4), the normalized active-rectifier dc-side voltage is

$$V_a^{pu}(\omega^{pu}) = \sqrt{2}\left(1+\alpha-\frac{3(1-k)\omega^{pu}}{\pi}\left(1-\frac{(\omega^{pu})^3 X_L^{pu}}{2(1+\alpha)}\right)\right) \tag{10}$$

where L_p in (8) is replaced by $(1-k)L$. The active-rectifier dc-side voltage must be greater than or equal to the corresponding ac port line-to-line back emf across the entire operating speed range. In per-unit form, this constraint is

$$V_a^{pu}(\omega^{pu}) \geq \sqrt{2}k\omega^{pu} \quad \forall \omega^{pu} \in [\omega_{min}^{pu}, 1]. \tag{11}$$

Equations (10) allows selection of a minimum α such that the constraint (11) is satisfied. For a given X_L^{pu} and minimum speed ω_{min}^{pu}, the split ratio k directly specifies α. As a consequence, the split ratio remains the only available design choice to minimize the power electronics VA-rating.

The next step is to calculate the active-rectifier rated voltage, rated current, and volt-ampere rating. The active rectifier must be rated for the maximum dc-side voltage across the whole operating speed range. The rated voltage is calculated by solving

$$V_{a,rated}^{pu} = \max_{\omega^{pu}\in[\omega_{min}^{pu},1]} V_a^{pu}(\omega^{pu}). \tag{12}$$

The active-rectifier ac-side current is dependent on the amount of power delivered to the dc-bus. Using the dq reference frame with the d axis aligned to the peak phase-A back emf, the power-balance relationship between the ac and the dc sides is

$$\frac{3}{2}E_{a,d}(\omega^{pu})I_{a,d}(\omega^{pu}) = V_a(\omega^{pu})I_{dc}(\omega^{pu}) \tag{13}$$

where $E_{a,d}$ and $I_{a,d}$ are the d-axis components of the ac voltage and current, respectively. Normalizing both sides by the product $V_{base}I_{base}$ and using $\frac{E_{a,d}}{V_{base}} = k\omega^{pu}\frac{\sqrt{2}}{\sqrt{3}}$ as well as (9), the active-rectifier d-axis current is

$$I_{a,d}^{pu}(\omega^{pu}) = \frac{(\omega^{pu})^2}{k(1+\alpha)}V_a^{pu}(\omega^{pu}). \tag{14}$$

$I_{a,d}^{pu}$ is the peak phase current when the q-axis current is set to zero for a unity power-factor operation. The maximum value of $I_{a,d}^{pu}$ is the active-rectifier rated current:

$$I_{a,rated}^{pu} = \max_{\omega^{pu}\in[\omega_{min}^{pu},1]} \frac{(\omega^{pu})^2}{k(1+\alpha)}V_a^{pu}(\omega^{pu}). \tag{15}$$

Using (12) and (15), the active-rectifier VA rating is minimized by selecting k as

$$\text{VA}_{rating}^{pu} = \min_{k\in[0,1]} V_{a,rated}^{pu} I_{a,rated}^{pu}. \tag{16}$$

The next design step is to specify the actual dc-bus voltage and the generator number of turns per phase. This specification requires V_{base}, which is set by the maximum actual voltage

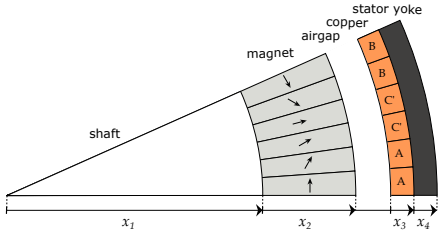

Figure 3. Geometric parameters used for optimization of the slotless generator.

that an active rectifier can provide, depending on the available power-electronic switch rating and converter topology. For example, a three-level neutral-point clamped active rectifier constructed from 4.5 kV-rated switches can handle a maximum dc-bus voltage of 9 kV. Allowing a 50% safety margin, such a rectifier could operated with $V_{a,rated} = 4.5$ kV. The base voltage is determined as

$$V_{base} = \frac{V_{a,rated}}{V_{a,rated}^{pu}}, \tag{17}$$

where $V_{a,rated}^{pu}$ is calculated using (12). Equations (3) and (7) are used to calculate the generator back emf E and V_{dc}, respectively, required by the power-electronics system. Lastly, the final generator design computes the number of turns per pole per phase N to match the generator back emf with the calculated E value.

III. Co-design example

This section uses the co-design framework to create a 10 MW, 9.6 r/min, direct-drive, integrated generator-rectifier system for an offshore wind turbine. The rated power and speed are chosen based on ongoing trend in the industry [10].

In the intial generator-design stage, a slotless topology with Halbach-array NdFeB magnets is being considered, as shown in Fig. 3. This topology can be designed to have a low inductance, which is preferred for the integrated generator-rectifier system to limit the imbalance in power processed by the active and the passive rectifiers. Four geometric variables are chosen to set up the multi-objective optimization along with their bounds, $x_1 ... x_4$, as shown in Table I. An airgap length of 10 mm is selected, because it is common at these power levels [4], [11]–[13]. Number of poles is selected to be 240. Boundaries for he shaft radius x_1 are picked to ensure the generator size does not exceed the transportation size limit. The current density limit J is chosen to ensure that forced air cooling is sufficient. A flux-density limit of 1.8 T is considered as the magnetic saturation limit. Each electromagnetic design is reinforced by a mechanical structure designed to have a gravitational airgap deflection less than 10% the nominal length and a torsional deflection of less than 0.05^o.

Figure 4(a) shows the optimization results for the initial generator-design stage. Each design point is accompanied by an X_L^{pu}, which is shown by the color bar. As expected, the feasible design space shows the classic trade-off between the generator efficiency and the active weight. The design points with lower X_L^{pu} use thicker magnets. Thus, the required current density is reduced to meet the rated power, which leads to a higher

Table I
Variable and constraints for slotless-NdFeB generators.

Variable	Notation	Unit	Lower bound	Upper bound
Shaft radius	x_1	mm	5000	6000
Magnet thickness	x_2	mm	10	70
Copper thickness	x_3	mm	25	100
Stator yoke thickness	x_4	mm	10	60
Current density	J	A/mm^2	1	4
Stator flux density	ψ_s	T	-	1.8

efficiency. For example, a feasible generator design could weigh 55 tons with a rated efficiency of 97%. In comparison, a conventional design weighs 67 tons with a 93.5% rated efficiency [4].

The next step is to design the power electronic converter for a compatible X_L^{pu}. From an active-rectifier topology selection perspective, a three-level neutral-point clamped converter is chosen to balance complexity and conversion efficiency. This topology is a typical industry choice for megawatt-scale power converter [14]. The selection of the minimum generator speed is an influencing parameter that trades off the active rectifier VA rating with the annual energy production. In the proposed co-design, the minimum speed is varied between 0.25 pu and 0.55 pu to capture this effect. The 0.25 pu value corresponds to the 3 m/s cut-in speed normalized by the 12m/s rated wind speed for a typical offshore wind site [15]. A typical minimum speed for a conventional DFIG system, which exhibits similar trade-offs [16], is 0.55 pu.

Three types of IGBTs are investigated for the active rectifier design: 3300 V, 4500 V, and 6500 V. A Simulink model is created to determined the voltage and current waveforms across each power electronics switch. These waveforms are combined with the losses characterization from the datasheet to estimate the conversion losses. The active-rectifier weight is estimated using a specific power of 0.55 kVA/kg [14]. The passive rectifier is assumed to have five times higher specific power. Fig. 4(b) shows the power electronics design in terms of weight and rated efficiency for a corresponding X_L^{pu}.

In contrast to a conventional trade-off characteristic between power density and efficiency in the power converter design, the proposed co-design shows a lower weight corresponding to a higher efficiency design. A lower-weight system is the result of a narrower operating speed range, which allows a higher dc-bus voltage. Therefore, the current required to deliver an identical power is reduced. The total conversion losses are lowered because the conduction loss is proportional to square of the current while the switching losses remain unchanged. For example, an attainable power-electronics design for any X_L^{pu} could exceed 99.5% conversion efficiency while weighing less than 15.5 tons. To put these numbers in perspective, a conventional, off-the-shelf, three-level full-power-rated converter has a conversion efficiency and weight of 97.9% and 22.7 tons, respectively [14].

The generator and power electronic designs for an identical

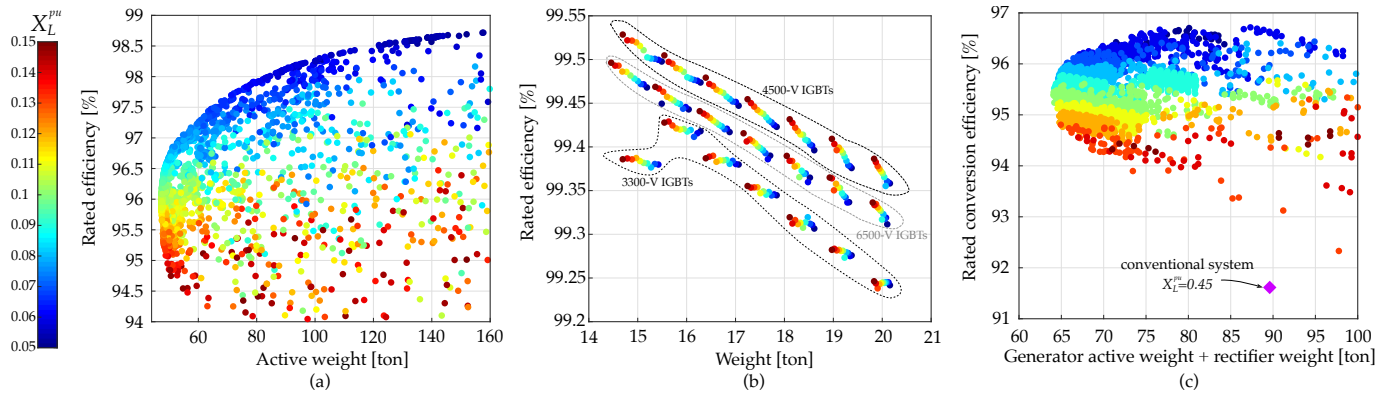

Figure 4. Weight versus efficiency characteristic of the designed (a) rectifiers, (b) generators, and (c) integrated system for different X_{pu}^{L} values.

X_L^{pu} are next assembled to compute the overall system weight and efficiency as illustrated in Fig. 4(c). Comparing the plausible designs of the proposed architecture with a reference design [4], shown by the diamond-purple marker, a reductions of 25 tons and a 61% conversion losses are achievable. As a final step for the co-design, the generator number of turns are computed for each attainable design point.

IV. Design Assessment

The ultimate goal for the electro-mechanical energy conversion system co-design is to minimize the LCOE of an offshore wind turbine. This section outlines the evaluation process for different feasible system design points in terms of annual energy production, reliability, and eventually LCOE. The assessment shows that the lowest LCOE design is not necessarily the design with maximum rated conversion efficiency or minimum weight.

A. Annual energy production

The electrical power output of a wind turbine as a function of the wind speed is essential for AEP calculation. The wind-turbine mechanical power depends on wind and rotational speeds, as illustrated in Fig. 5 for a 10-MW wind turbine. At each wind speed, the maximum mechanical power should be extracted. For a direct-drive system, maximum power extraction requires the per-unit generator speed and per-unit wind speed to be identical, as marked by the green stars in Fig. 5. In an integrated generator-rectifier system, the minimum generator speed may not be identical with the per-unit cut-in wind speed, because expanding the speed range increases the volt-ampere rating of the active rectifier [5]. A minimum generator speed should be judiciously selected to balance the rectifier cost and additional benefits of extending the speed range. When the wind speed is lower than minimum generator speed, the generators must be forced to rotate at the minimum speed and extract the amount of power marked by orange stars in Fig. 5.

The generator and rectifier conversion efficiency translates available mechanical power to electrical-power output. At partial-speed conditions, conversion efficiency is different from that at the rated condition. For example, Fig. 6 illustrates the conversion efficiencies of rectifiers and generators with a speed

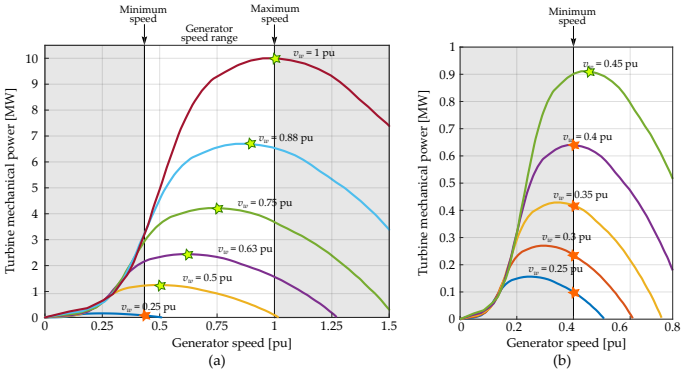

Figure 5. (a) Mechanical power versus rotational speed of a 10-MW wind turbine. (b) Magnified section of the mechanical power at low wind speeds. The wind speed is normalized by the rated value, typically 12 m/s for offshore wind.

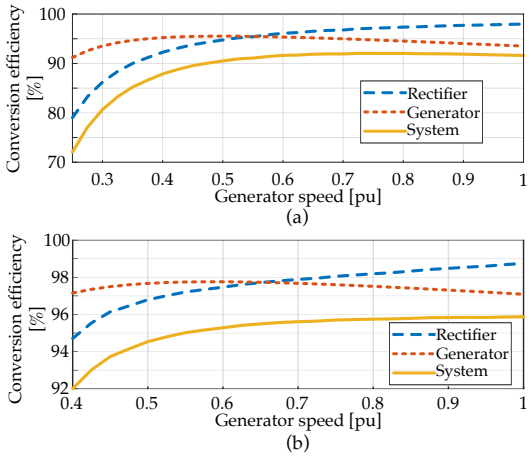

Figure 6. Conversion efficiency of (a) a conventional full-power-rated rectifier [4], and (b) a sample design of the integrated generator-rectifier system as a function of generator speed.

range from 0.4 to 1 pu for a typical conventional system and an integrated generator-rectifier system. The product of the power electronics and the generator efficiency curves is the system mechanical-to-electrical power conversion efficiency, as illustrated by the solid-yellow curves.

Information about wind-speed probability distribution is

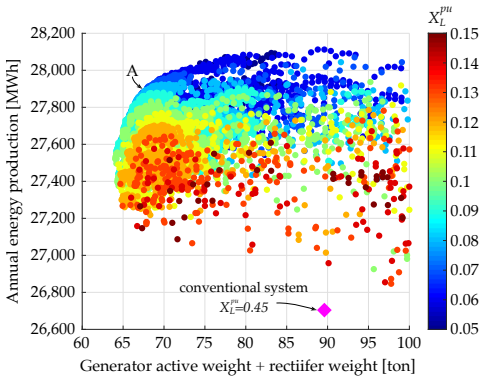

Figure 7. Annual energy production of the integrated generator-rectifier system and the conventional system based on a wind profile from Buoy 44028, off the coast of Massachusetts [15].

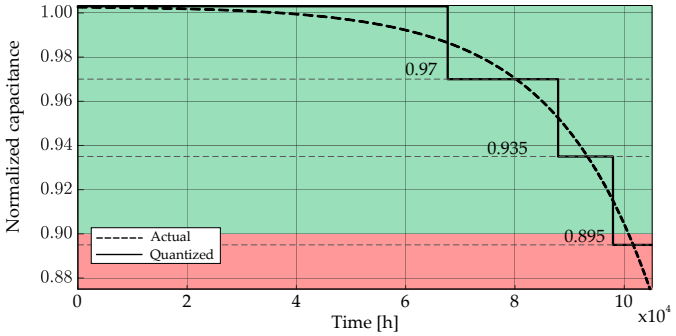

Figure 8. Capacitance degradation curve using model in [17] being modified to match the life expectancy reported in [18]. Quantization ensuring a maximum 2% error between the quantized and the actual capacitance is applied to create a stair-case degradation characteristic for reliability analysis.

essential for the AEP computation. As an example, the wind-speed probability of the Buoy 44028, off the coast of Massachusetts is used [15]. Annual energy production ϵ is calculated by

$$\epsilon = A_v \mathbb{E}\big[P_e(v_w)\big], \tag{18}$$

where A_v is the wind turbine availability, $\mathbb{E}$ is the expected value operator, P_e is the output electrical power as a function of wind speed v_w. Fig. 7 shows the AEP based on the integrated generator-rectifier systems assuming $A_v = 1$. For the same weight, the integrated generator-rectifier system could increase the annual energy production by 5.2% compared to the conventional system, from 26,700 MWh/year to 28,100 MWh/year. At point A on the Pareto front, the total weight is reduced by 25%, from 89 to 67 tons, while the energy yield is increased by 4.5%, from 26,700 MWh/year to 27,900 MWh/year.

B. System reliability

Improvement in the reliability of the electromechanical drive train and the power converter lowers the operational and maintenance cost as well as improves system availability. This subsection evaluates the reliability of the integrated generator-rectifier system using the failure rate metric. The generator is much more reliable compare its power electronics. Therefore, failure rate of the serially connected passive and active rectifiers represents that of the integrated generator-rectifier system.

The integrated generator-rectifier system comprises three passive rectifiers and one active rectifier for total generator power-flow control. Each passive rectifier comprises six line-frequency diodes. The active rectifier has six IGBTs and a dc-link film capacitor. The integrated generator-rectifier system is in a failed state when one or more diodes fails, one or more active switches fails (e.g., due to gate-drive or device failures), or the film capacitor's capacitance degrades by 10 percent, or more, of the nominal value. While failures of the diodes and the IGBTs are binary, the capacitor is assumed to take intermediate values before reaching the end of life, as illustrated in Fig. 8.

Fig. 9 illustrates the Markov reliability model state-transition diagram for the integrated generator-rectifier systems. The model captures four failure events and seven possible configurations as listed in the associated tables. The system initially stays in configuration 1. If at least one diode of the 18 diodes

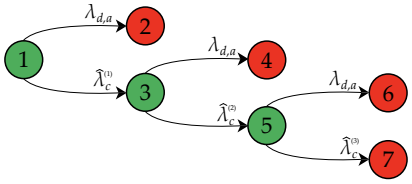

Event	Description	Failure rate
D	at least 1 of 18 diodes fails	$18\lambda_d$
AS	at least 1 of 6 active switches fails	$6\hat{\lambda}_{as}$
C1	capacitor degrades to 0.97 of its nominal value	$\hat{\lambda}_c^{(1)}$
C2	capacitor degrades to 0.935 of its nominal value	$\hat{\lambda}_c^{(2)}$
C3	capacitor degrades to 0.895 of its nominal value	$\hat{\lambda}_c^{(3)}$

Configuration	Failure sequence	Probability
1	{∅}	$\pi_1(t)$
2	{D} or {AS}	$\pi_2(t)$
3	{C1}	$\pi_3(t)$
4	{C1→D} or {C1→AS}	$\pi_4(t)$
5	{C1→C2}	$\pi_5(t)$
6	{C1→C2→D} or {C1→C2→AS}	$\pi_6(t)$
7	{C1→C2→C3}	$\pi_7(t)$

Figure 9. Markov reliability model state-transition diagram for the proposed converter architecture. Green states indicate sequences of failures in which the converter is operational. Red states indicate sequences of failures in which the converter is not operational.

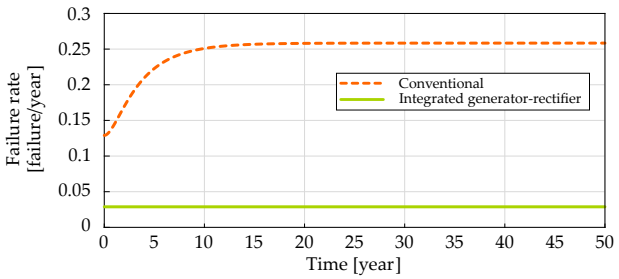

Figure 10. Compared to the conventional system (dash-orange) curve, an integrated generator-rectifier has a significantly lower failure rate (solid-green curve). The long-term rate is reduced by 9x.

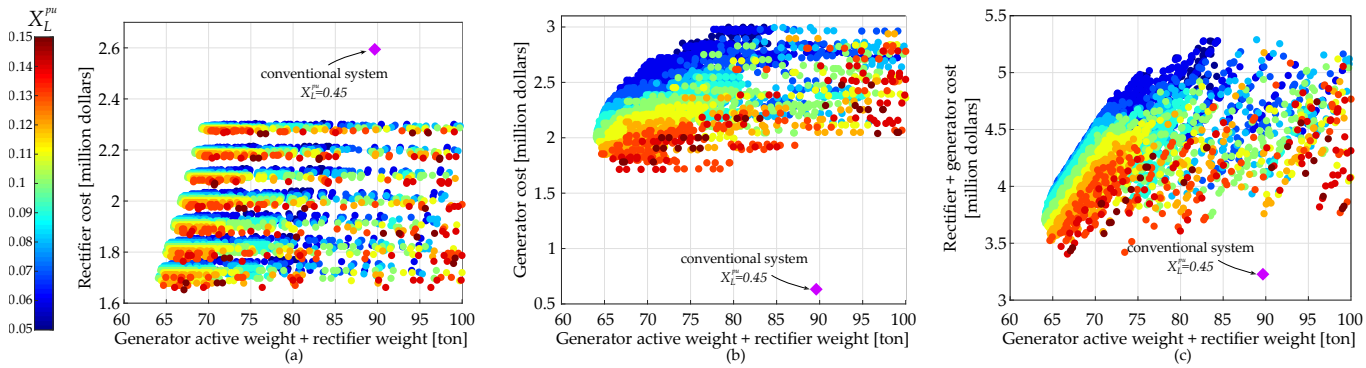

Figure 11. Integrated generator-rectifier systems leads to (a) lower power electronics cost, but (b) higher generator cost, and (c) higher overall system cost.

Table II
COMPONENT FAILURE RATES IN A CONVENTIONAL [19]–[21] AND AN INTEGRATED GENERATOR-RECTIFIER SYSTEM [22].

Failure rate [failures/year]	Conventional	Integrated generator-rectifier
λ_d	0	0.0016
λ_{as}	0.0215	3.36×10^{-4}
$\hat{\lambda}_c^{(1)}$	0.1294	0.002
$\hat{\lambda}_c^{(2)}$	0.4334	0.0068
$\hat{\lambda}_c^{(3)}$	0.8725	0.0136

or one of 6 IGBTs fails, the system enters configuration 2 with a transition rate:

$$\lambda_{d,a} = 18\lambda_d + 6\hat{\lambda}_{as} \tag{19}$$

where λ_d is the diode failure rate and $\hat{\lambda}_{as}$ is the IGBT failure rate. The transition from configuration 3 to 4 and from state 5 to 6 is caused by the same mechanism. The transition from configuration 1 to 3 and configuration 3 to 5 are characterized by a degraded but not yet end-of-life capacitor. The transition rates are denoted by $\hat{\lambda}_c^{(1)}$ and $\hat{\lambda}_c^{(1)}$, respectively. The transition from configuration 5 to 7 is caused by the capacitor reaching its end-of-life. The transition rate is denoted by $\hat{\lambda}_c^{(3)}$.

The Chapman-Kolmogorov equation is used to evaluate probability of the system in each configuration as a function of time. The equation is

$$\dot{\boldsymbol{\pi}} = \mathbf{A}\boldsymbol{\pi} \tag{20}$$

where $\boldsymbol{\pi} = [\pi_1, \pi_2, \pi_3, \pi_4, \pi_5, \pi_6, \pi_7]^T$ with π_i being the probability of the system to stay in the configuration i-th, and $\mathbf{A}$ is the transition matrix constructed from Fig. 9.

The probability that the integrated generator-rectifier system remains operational at time t is

$$\begin{aligned}\Pr\{T > t\} &= \Pr\{\text{active rectifier is operational at time } t\} \\ &= \pi_1(t) + \pi_3(t) + \pi_5(t).\end{aligned} \tag{21}$$

where T is a random variable describing the time to failure. The cumulative density function $F_T(t)$ and probability density function $f_T(t)$ are

$$F_T(t) = 1 - \pi_1(t) - \pi_3(t) - \pi_5(t), \tag{22}$$

$$f_T(t) = -\dot{\pi}_1(t) - \dot{\pi}_3(t) - \dot{\pi}_5(t). \tag{23}$$

The system failure rate is

$$\begin{aligned}\lambda_{pa}(t) &= \frac{f_T(t)}{1 - F_T(t)} \\ &= \frac{(\pi_1(t) + \pi_3(t) + \pi_5(t))\lambda_{d,a} + \pi_5(t)\hat{\lambda}_c^{(3)}}{\pi_1(t) + \pi_3(t) + \pi_5(t)}.\end{aligned} \tag{24}$$

The first equality is the definition and the second is achieved by substitution of (20), (22) and (23) into the definition.

Fig. 10 compares the failure rate λ_{pa} versus time between the integrated generator-rectifier and the conventional system, showing a 9x reduction in the long term rate. Parameters for calculation are listed in Table II. Over a long time period of twenty years, the integrated generator-rectifier system fails 0.6 times while the conventional system has 4.7 failures. Parameter values for the conventional system are extracted from references [19]–[21]. The diode failure rate is zero due to absence of the passive rectifiers. For the integrated generator-rectifier system, the diode failure rate is 0.0016 failure/year, typical for a high-power line-frequency diode [22]. The component failure rates corresponding to the active rectifier are assumed to be 0.25^3 times the values of a conventional system because the active rectifier processes approximately 25% of the total power in a 4-port configuration [5], [21].

C. LCOE

For comparison, LCOE is calculated at the 10 MW power level. The fixed cost c_f is calculated by adjusting the reference number in [4] by the generator and rectifier cost variation. Fig. 11 compares the costs of integrated generator-rectifier and conventional systems. While the power electronics has a lower cost, the generator is more expensive. However, the generator cost in a wind turbine is merely 9% of the overall cost [4]. Therefore, increasing the generator cost to reduce active-material weight and improved efficiency has the potential to translate into lower LCOE. A lighter system has the potential to reduce the supporting structure requirement, which shares the largest cost in a wind turbine [4]. The O&M cost of the integrated generator-rectifier system is that of the conventional system with the shares belonging to the drive train and generator scaled linearly by the failure rate in the twentieth year, as calculated in Section IV-B. Additionally, the integrated generator-rectifier is assumed to have an availability of 98% compared to 94% for the conventional system due to

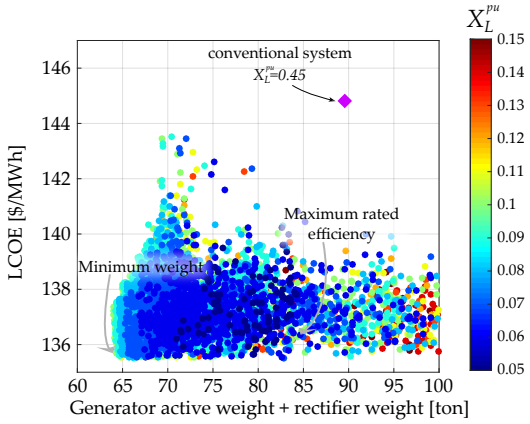

Figure 12. Integrated generator-rectifier leads to lower LCOE compared to the conventional system.

Table III
PARAMETERS FOR LCOE CALCULATION

Parameter	Conventional	Integrated generator-rectifier	Unit
φ	0.108	0.108	–
O&M cost density	62.59	58.55	$/kW/year
A_v	0.94	0.98	–

a lower failure rate. A capital recovery factor of 0.108 is used. The parameter values for LCOE calculation are summarized in Table III.

Fig. 12 compares the LCOE values. As a conservative estimate, the integrated generator-rectifier system could bring the LCOE to approximately 135.5 $/MWh compared to 145 $/MWh of a conventional system. The reduction is mostly attributed to higher conversion efficiency and availability as well as lower O&M costs. The estimation assumes unchanged tower and foundation costs. The benefits would be more substantial if effects of the weight reduction on the supporting structure is considered.

V. CONCLUSIONS

This paper discusses the co-design framework for the integrated generator-rectifier system. Due to the inter-dependency between the power electronics and the generator through X_L^{pu}, such a framework is necessary to ensure the active-rectifier size is minimal while the generator is optimized for weight and efficiency. Illustrative example shows the output designs could reduce the weight by 25% and the conversion losses by 61%. Assessments based on AEP, failure rate, and LCOE are also presented. The integrated generator-rectifier system could increase the annual energy output by 4.5%, reduce the long-term failure rate by 9x, and consequently curb the LCOE by 6.5%. These improvements make integrated generator-rectifier system well suited for offshore wind energy harvesting.

VI. ACKNOWLEDGMENT

The information, data, or work presented herein was supported by the Advanced Research Projects Agency-Energy (ARPA-E), U.S. Department of Energy, under Award DE-AR0001057. The authors would also like to thank the Grainger Center for Electric Machinery and Electromechanics for partially funding this project.

REFERENCES

[1] D. S. Ottensen, "Global offshore wind market report," Norweigian Energy Partner, Tech. Rep., 2018.
[2] EIA, "Levelized cost and levelized avoided cost of new generation resources in the annual energy outlook 2018," U.S. Energy Information Adminstration, Tech. Rep., 2018. [Online]. Available: https://www.eia.gov/outlooks/aeo/pdf/electricity_generation.pdf
[3] V. Yaramasu, B. Wu, P. C. Sen, S. Kouro, and M. Narimani, "High-power wind energy conversion systems: State-of-the-art and emerging technologies," *Proceedings of the IEEE*, vol. 103, no. 5, pp. 740–788, May 2015.
[4] L. Sethuraman, M. Maness, and K. Dykes, "Optimized generator designs for the DTU 10-MW offshore wind turbine using GeneratorSE," in *35th Wind Energy Symposium*, 2017, p. 0922.
[5] P. T. Huynh, P. J. Wang, and A. Banerjee, "An integrated permanent-magnet-synchronous generator–rectifier architecture for limited-speed-range applications," *IEEE Transactions on Power Electronics*, vol. 35, no. 5, pp. 4767–4779, 2020.
[6] P. T. Huynh and A. Banerjee, "Active voltage-ripple compensation in an integrated generator-rectifier system," *IEEE Transactions on Power Electronics*, pp. 1–1, 2020.
[7] P. T. Huynh, S. Tungare, and A. Banerjee, "Maximum power point tracking for wind turbine using integrated generator-rectifier systems," *IEEE Transactions on Power Electronics*, pp. 1–1, 2020.
[8] S. Sudhoff, "Genetic Optimization System Engineering Tool (GOSET) For Use with MATLAB, Manual Version 2.4, School of Electrical and Computer Engineering, Purdue University, West Lafayette, IN with United States Naval Academy, Annapolis, MD, 2005."
[9] J. G. Kassakian, M. F. Schlecht, and G. C. Verghese, *Principles of Power Electronics*. Addison-Wesley Publishing Company, 1991.
[10] C. Bak, F. Zahle, R. Bitsche, T. Kim, A. Yde, L. C. Henriksen, M. H. Hansen, J. P. A. A. Blasques, M. Gaunaa, and A. Natarajan, "The DTU 10-MW reference wind turbine," in *Danish Wind Power Research 2013*, 2013.
[11] K. O. Merz, "Dogger bank reference wind power plant: Layout, electrical design, and wind turbine specification," SINTEFF Energy Research, Tech. Rep., 2016.
[12] H. Polinder, D. Bang, R. Van Rooij, A. McDonald, and M. Mueller, "10 mw wind turbine direct-drive generator design with pitch or active speed stall control," in *2007 IEEE International Electric Machines & Drives Conference*, vol. 2. IEEE, 2007, pp. 1390–1395.
[13] Y. Duan and R. G. Harley, "Present and future trends in wind turbine generator designs," in *2009 IEEE Power Electronics and Machines in Wind Applications*, June 2009, pp. 1–6.
[14] Toshiba, "T300MVi/MTX medium-voltage adjustable-speed motor drive," Available: https://www.toshiba.com/tic/datafiles/manuals/IF08CZ00_T300MVi-MTX_Instruction_Manual_3-31-2012_7437.pdf [Accessed: Dec. 28, 2019].
[15] E. C. Morgan, M. Lackner, R. M. Vogel, and L. G. Baise, "Probability distributions for offshore wind speeds," *Energy Conversion and Management*, vol. 52, no. 1, pp. 15 – 26, 2011. [Online]. Available: http://www.sciencedirect.com/science/article/pii/S019689041000227X
[16] R. Pena, J. C. Clare, and G. M. Asher, "Doubly fed induction generator using back-to-back pwm converters and its application to variable-speed wind-energy generation," *IEE Proceedings - Electric Power Applications*, vol. 143, no. 3, pp. 231–241, May 1996.
[17] H. Wang, D. A. Nielsen, and F. Blaabjerg, "Degradation testing and failure analysis of dc film capacitors under high humidity conditions," *Microelectronics Reliability*, vol. 55, no. 9, pp. 2007 – 2011, 2015.
[18] *DC Link Film capacitors Datasheets*, Mouser Electronics. [Online]. Available: https://www.mouser.com/Passive-Components/Capacitors/Film-Capacitors/Datasheets/_/N-9x371?P=1yzvdnf
[19] J. Carroll, A. McDonald, and D. McMillan, "Reliability comparison of wind turbines with DFIG and PMG drive trains," *IEEE Transactions on Energy Conversion*, vol. 30, no. 2, pp. 663–670, June 2015.
[20] J. Angus and A. Ward, *Electronic Product Design*, ser. Tutorial guides in electronic engineering. Taylor & Francis, 1996.
[21] I. Bazovsky, *Reliability Theory and Practice*, ser. Dover Civil and Mechanical Engineering Series. Dover Publications, 2004.
[22] *Vishay Semiconductors*, Vishay. [Online]. Available: https://www.vishay.com/